BIOCHEMISTRY
including biophysical chemistry & molecular biology

Article

pubs.acs.org/biochemistry

Helix-Dipole Effects in Peptide Self-Assembly to Amyloid

Gai Liu, Kevin J. Robbins, Samuel Sparks, Veli Selmani, Kalin M. Bilides, Erin E. Gomes, and Noel D. Lazo*

Carlson School of Chemistry and Biochemistry, Clark University, 950 Main Street, Worcester, Massachusetts 01610, United States

Supporting Information

ABSTRACT: The formation of amyloid fibrils is associated with incurable diseases including Alzheimer's, Parkinson's, and type 2 diabetes. Important mechanistic details of the self-assembly are unknown partly because of the absence of a clear structural characterization of intermediates. There is experimental evidence, however, for α-helical intermediates that has come primarily from circular dichroism spectroscopy. Here, we strengthen the evidence for helical intermediates by demonstrating helix-dipole effects in the early events of self-assembly. Previously, we showed that capped peptides containing the part of the islet amyloid polypeptide that may be responsible for the initial intermolecular contacts (Acetyl-R_{11}LANFLVHSSNNFGA$_{25}$-NH_2 and Acetyl-R_{11}LANFLVHSGNNFGA$_{25}$-NH_2 which contains the S20G mutation associated with early onset type 2 diabetes) self-assemble via helical intermediates [Liu et al. (2010) *J. Am. Chem. Soc. 132*, 18223−18232]. We demonstrate here that when the peptides are uncapped, they do not self-assemble as indicated primarily by circular dichroism and nuclear magnetic resonance data. Self-assembly is restored when the charge on α-NH_3^+ of Arg11 is eliminated but not when the charge on α-COO^- of Ala25 is removed, consistent with the helicity of the peptides skewed toward the N-terminus. Our results strengthen the hypothesis that α-helical intermediates are on pathway to amyloid formation and indicate that the helix dipole is an attractive target for inhibiting the formation of α-helical assemblies.

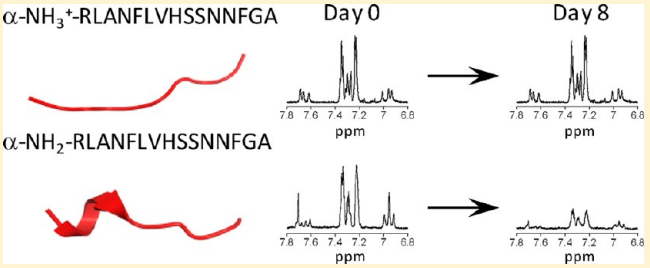

Amyloid fibrils are present in diseased organs in Alzheimer's disease (AD), Parkinson's disease (PD), Huntington's disease (HD), and type 2 diabetes (T2D).[1] Because of this and *in vitro* studies indicating that both oligomeric precursors[2−7] and fibrils[8−10] are toxic, the elucidation of the mechanism of self-assembly starting from the monomeric protein to intermediates and then to the mature fibril is of high biomedical and biophysical interest. Achieving this has been challenging due in part to the fleeting nature of intermediates making structural characterization difficult. Nevertheless, studies of the self-assembly of the amyloid-β protein (Aβ) in AD, α-synuclein (α-syn) in PD, islet amyloid polypeptide (IAPP) in T2D, and the huntingtin protein in HD have shown that α-helical assemblies may be on pathway to amyloid formation.[11−17] The evidence for the helical intermediates is based primarily on circular dichroism (CD) spectroscopy used to identify changes in secondary structure with time. CD spectroscopy is sensitive to α-helix.[18] But when the helix content is low and some β-sheet and random coil are present, as may be the case in amyloid formation, the spectral contribution of the α-helix may be swamped out, making helix detection and accurate quantification of helix content difficult. Also, light scattering by assemblies and the absence of suitable reference databases make deconvolution of CD spectra for secondary structure distribution unreliable.[16] Nuclear magnetic resonance (NMR) is also sensitive to α-helix.[19] However, the helical intermediates are too large and convert to larger assemblies rapidly for NMR to be useful.[16,20]

If α-helical assemblies are on pathway to amyloid formation, helix destabilization should delay or inhibit self-assembly. One way to destabilize the α-helix is through helix-dipole effects. The helix dipole originates from the alignment of the dipole moments of the individual peptide bonds resulting in a positive and negative charge in the N- and C-termini of an α-helix composed of one or more turns (Figure 1).[21,22] Thus, a positive charge at the helix N-terminus or a negative charge at the helix C-terminus is destabilizing. Indeed, helical peptides with charged ends linked to uncapped or free termini are predominantly random coil.[23−25] When the charged ends are removed by chemical means, e.g., acetylation and amidation of the N- and C-termini, respectively, or by pH titration, the peptides become predominantly α-helix.[23−25]

In the past few years, our laboratory has focused on the self-assembly of the islet amyloid polypeptide (IAPP), associated with the death of pancreatic β-cells in T2D.[7] Using limited proteolysis combined with mass spectrometry, we have previously identified the segment containing residues 11−25 as involved in the initial intermolecular interactions.[16] Interestingly, a capped peptide containing this part (cWT, Figure 2) forms transient monomeric α-helices as indicated by NMR and self-assembles via helical intermediates as suggested by CD.[16] When a serine-to-glycine substitution was made at

Received: October 17, 2011
Revised: May 3, 2012
Published: May 4, 2012

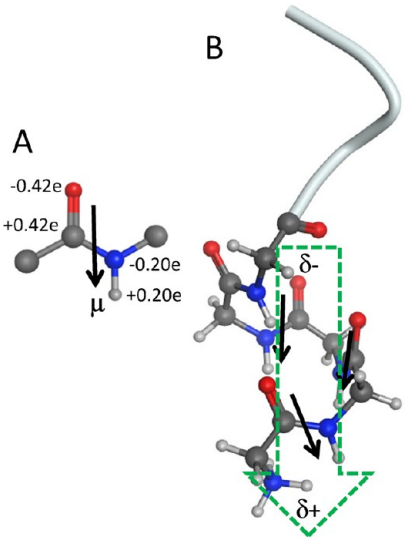

Figure 1. (A) Partial charges on CO and NH in the peptide bond result in a dipole moment μ.[22] (B) In one helix turn, the dipole moments μ (black arrows) align, resulting in a helix dipole (green arrow) which has a partial positive charge at the N-terminus and a partial negative charge at the end of the helix turn.

Capped

cWT Acetyl-R_{11}L A N F L V H S S N N F G A_{25}-NH_2

↓

cS20G Acetyl-R_{11}L A N F L V H S *G* N N F G A_{25}-NH_2

Uncapped

uWT NH_3^+-R_{11}L A N F L V H S S N N F G A_{25}-COO^-

↓

uS20G NH_3^+-R_{11}L A N F L V H S *G* N N F G A_{25}-COO^-

Half-capped

Ac-S20G Acetyl-R_{11}L A N F L V H S *G* N N F G A_{25}

S20G-NH_2 R_{11}L A N F L V H S *G* N N F G A_{25}-NH_2

Figure 2. Capped, uncapped, and half-capped peptides containing residues 11−25 of IAPP. The capped peptides cWT and cS20G are acetylated and amidated in the N- and C-terminus, respectively. The uncapped peptides uWT and uS20G will have charged ends at pH 3−8, i.e., α-NH_3^+ and α-COO^-. Titratable residues include arginine at position 11 and histidine at position 18. The serine-to-glycine substitution at position 20 is associated with increased amyloidogenicity of IAPP and early onset type 2 diabetes.[26,27] Half-capped IAPP(11−25) peptides containing the S20G mutation include Ac-S20G and S20G-NH_2.

position 20, a mutation associated with increased amyloidogenicity of IAPP and early onset T2D,[26,27] the capped peptide (cS20G, Figure 2) aggregated at a faster rate than cWT and formed amyloid fibrils similar to those formed by full-length IAPP.[16]

Here, we synthesized uWT and uS20G (Figure 2), uncapped counterparts of cWT and cS20G, and then determined their competence for self-assembly at conditions when both ends of the peptides are charged and also when only one end is charged. Our results show that the uncapped peptides do not self-assemble. Self-assembly is restored when the charge on α-NH^{3+} of Arg11 is removed by acetylation or by pH titration. Together, our results provide evidence for the importance of helix dipole effects in the early events of self-assembly. We discuss insights into the mechanism of self-assembly thus obtained.

MATERIALS AND METHODS

Peptide Synthesis. Capped, uncapped, and half-capped IAPP(11−25) peptides (Figure 2) were synthesized in-house by standard 9-fluorenylmethoxycarbonyl (FMOC) chemistry using an Applied Biosystems 433A peptide synthesizer. All FMOC-protected amino acids and resins were purchased from EMD Chemicals. To make amidated peptides, NovaPEG Rink amide resin LL (low loading) was used. Peptides with free C-termini were synthesized using FMOC-Ala-NovaSyn TGT resin. Acetylation was accomplished by coupling acetic acid after Arg11. After cleavage from the resin, all peptides were purified by reverse-phase HPLC. The identities of the peptides were confirmed by electrospray ionization mass spectrometry at the University of Massachusetts Medical School.

Preparation of Samples for Biophysical Studies. Aggregate-free peptide stock solutions were prepared as described elsewhere.[16] Briefly, dry purified peptide was dissolved in ice-cold 10 mM sodium phosphate buffer (pH 2.0, 4.3, 7.0 or 10.0). In order to remove undissolved peptide and preformed aggregates, the solutions were centrifuged at 16000*g* for 30 s followed by a careful transfer of the supernatant into an Eppendorf tube. This procedure was repeated three times. Peptide concentrations were determined by UV absorbance at 214 nm as described elsewhere[16] and by amino acid analysis at the Keck Amino Acid Analysis and Protein Sequencing Laboratory of Yale University.

To calculate the percentage of base and protonated species as a function of pH for all titratable residues, we used eq 1, which can be easily derived from the Henderson−Hasselbalch equation.

$$[\text{base}]\% = \frac{10^{\text{pH}-\text{p}K_a}}{10^{\text{pH}-\text{p}K_a}+1} \times 100 \quad (1)$$

Dot Blot Assay. Two microliters of the peptide sample was spotted onto nitrocellulose membranes, air-dried, and then blocked with 10% nonfat milk in Tris-buffered saline with Tween-20 (TBST) at 4 °C for 1 h. After washing with TBST, the membrane was then probed with the antioligomer antibody A11 (Invitrogen) diluted in 5% nonfat dry milk in TBST (1:10 000) for 12 h at 4 °C. After incubation with the secondary antibody solution (goat anti-mouse horseradish peroxidase-conjugated antibody diluted in 5% nonfat dry milk in TBST (1:10 000)) for 1 h at 4 °C, the membrane was developed using Novex ECL chemiluminescent substrate reagent kit (Invitrogen).

Circular Dichroism (CD). All CD spectra were acquired at 4 °C using a JASCO J-815 spectropolarimeter. Stoppered quartz cuvettes with a path length of 1 mm were used in all acquisitions. All spectra are averages of 4 scans, each recorded using a 1 nm bandwidth and an averaging time of 4 s. To minimize sample perturbation, the peptide solutions were incubated in the CD cuvettes. All samples were stored at 4 °C in between data acquisition.

Because of the absence of suitable reference databases, algorithms which have been used widely for the deconvolution of CD spectra of monomeric proteins may not work for

dx.doi.org/10.1021/bi3001616 | *Biochemistry* 2012, 51, 4167−4174

amyloidogenic peptides or proteins.[16,28] An alternative approach to determine α-helix content is to use eq 2:[29]

$$\text{helix \%} = \frac{[\theta]_{222}(\text{obs})}{[\theta]_{222}(100\%\ \text{helix})} \times 100 \quad (2)$$

where $[\theta]_{222}$(100% helix) is calculated using eq 3:[29]

$$[\theta]_{222}(100\%\ \text{helix}) = X_{\text{H}}^{\infty}\left(1 - \frac{k}{n}\right) \quad (3)$$

in which X_{H}^{∞} is the molar ellipticity for an infinite helix assumed to be equal to −43 000 deg cm^2 dmol^{-1},[30] k is the wavelength-dependent factor at 222 nm equal to 2.5,[29] and n, the number of residues, is equal to 15. Using eq 3, $[\theta]_{222}$(100% helix) is equal to −36 000 deg cm^2 dmol^{-1}.

Transmission Electron Microscopy (TEM). Aliquots taken from CD samples on day 8 were placed on carbon-coated copper grids and incubated for 2 min, followed by staining with 1% uranyl acetate. TEM was performed at the Core Electron Microscopy Facility of the University of Massachusetts Medical School.

Thioflavin T (ThT) Fluorescence. After 8 days of incubation, aliquots of the CD samples were taken and diluted with the appropriate phosphate buffer to give a final peptide concentration of 20 μM. Aliquots of a ThT stock solution (ThT concentration ∼240 μM) were then added to these solutions so that all samples contained 20 μM of ThT. Fluorescence was measured using a Perkin-Elmer LS50B luminescence spectrometer. The excitation wavelength was set at 440 nm. Emission spectra were recorded from 450 to 600 nm. The slit width for both excitation and emission was set at 10 nm.

Nuclear Magnetic Resonance (NMR) Spectroscopy. One-dimensional (1D) and two-dimensional (2D) ^{1}H NMR spectra were recorded at 4 °C on a 600 MHz Varian INOVA spectrometer. Water suppression was achieved by presaturation and WATERGATE in the 1D and 2D NMR experiments, respectively. TOCSY (total correlation spectroscopy) spectra were acquired with a mixing time of 80 ms using the MLEV-17 spin-lock sequence.[31] ROESY (rotating-frame Overhauser enhancement spectroscopy) and NOESY (nuclear Overhauser effect spectroscopy)[31] spectra were obtained for sequential peak assignments using a mixing time of 300 ms. All chemical shifts were referenced relative to the methyl resonance of 2,2-dimethyl-2-silapentane-5-sulfonate (DSS) at 0 ppm. To calculate secondary chemical shifts ($\Delta\delta = \delta_{\text{observed}} - \delta_{\text{random coil}}$)[32] of the H$^\alpha$ protons, we used the database derived random coil shift averages found in the Biological Magnetic Resonance Data Bank. We note in Table S1 that the averages compare well with the random coil data corrected for sequence effects obtained by Schwarzinger et al.[33] To study the kinetics of aggregation, a series of 1D and TOCSY spectra were collected. Peak areas and peak volumes in the 1D and TOCSY spectra, respectively, relative to the area or volume of the methyl peak of DSS, which does not change with self-assembly of the peptides, were determined and then plotted as a function of time. All samples were stored at 4 °C in between acquisition of spectra.

RESULTS AND DISCUSSION

Uncapped Analogues of Amyloidogenic Peptides Which Self-Assemble via Helical Intermediates Do Not Aggregate at pH 4.3. We determined the competence of uWT and uS20G for self-assembly at conditions used previously in studies of cWT and cS20G, i.e., pH 4.3 and 4 °C.[16] At pH 4.3, both the α-amino of Arg11 (pK_a 8.2)[24] and α-carboxyl of Ala25 (pK_a 3.2)[24] are charged. Far UV circular dichroic (CD) spectra of uS20G (Figure 3A) and uWT (Figure S1A) did not change with incubation time. TOCSY spectra of uS20G (Figure 3B) and uWT (Figure S1B) acquired after 20 days of incubation were essentially identical to spectra recorded

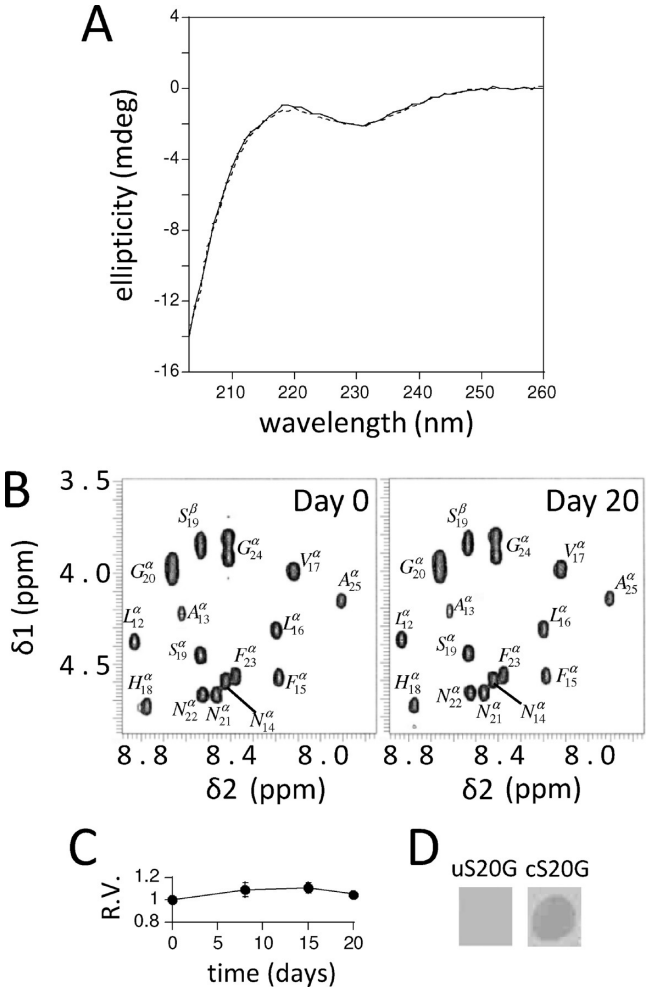

Figure 3. Self-assembly of cS20G is abolished by removal of the terminal capping groups. (A) Conformational transitions associated with amyloid formation were not observed in far-UV CD spectra of uS20G. The spectrum acquired 20 days after sample preparation (dotted line) is essentially identical to the spectrum recorded immediately after sample preparation (solid line). (B) The TOCSY spectrum acquired immediately after sample preparation is essentially identical to that recorded after 20 days of incubation. Peak broadening indicative of aggregation or new signals suggesting the presence new species was not observed in the day 20 spectrum. (C) Signal loss consistent with self-assembly was not observed in NMR spectra acquired over time. The sum of the relative peak volumes (RV) of the NH → H$^\alpha$ cross-peaks in TOCSY spectra acquired at day 0, day 8, day 15, and day 20 did not change significantly, consistent with the absence of self-assembly. (D) Oligomers were not detected by a biochemical assay. Dot blot assay of the 20 day old uS20G sample using the antioligomer antibody A11 shows the absence of oligomers. Peptide cS20G, which self-assembles rapidly, was used as positive control. The peptide concentration of CD and NMR samples is ∼60 μM.

dx.doi.org/10.1021/bi3001616 | Biochemistry 2012, 51, 4167−4174

immediately after sample preparation. In particular, the volumes of NH → H^{α} cross-peaks, which decrease with self-assembly,[16] did not change significantly with incubation time (see Figure 3C for uS20G and Figure S1C for uWT). Dot blot assays of solutions of uS20G (Figure 3D) and uWT (Figure S1D) probed by the antioligomer antibody A11[34] showed negative results for oligomers. Together, our results indicate that the uncapped peptides do not self-assemble, in sharp contrast to the capped peptides.

A possible explanation for the absence of aggregation by the uncapped peptides is the formation of folded, stable, monomeric structures that render the peptides incompetent for self-assembly. These structures may be stabilized by an intramolecular electrostatic attraction between the positively charged N-terminus and the negatively charged C-terminus. However, we did not observe long-range rotating-frame Overhauser enhancements (ROEs) that would indicate that Arg11 or Leu12 is close in space to Gly24 or Ala25 (Figures S2 and S3). We also considered a structure that would be stabilized by an electrostatic attraction between the positively charged His18 side chain and the negatively charged C-terminus. No ROEs between His18 and C-terminal residues were observed (Figures S4 and S5). Clearly, the absence of self-assembly by the uncapped peptides cannot be explained by the formation of folded, aggregation-incompetent monomeric structures.

Self-Assembly of the Uncapped Peptides Is Restored at pH 10.0 but Not at pH 2.0 or 7.0. In order to isolate the effect of the α-NH_3^+ group from that of the α-COO^- group, we then tested for self-assembly of the uncapped peptides at pH 2.0 and pH 10.0. At pH 2.0, the α-COO^- of Ala25 is protonated to a neutral species, i.e., α-COOH (94% from eq 1). At this pH, CD and NMR spectra of uS20G (Figures 4A and 4B, respectively) and uWT (Figure S6) acquired over time indicate the absence of self-assembly. Line broadening or decrease in peak intensity in the ^{1}H NMR spectra indicative of self-assembly was not observed in the backbone amide and methyl regions, the two regions most sensitive to aggregation. At pH 10.0, the α-NH_3^+ of Arg11 is deprotonated to a neutral species, i.e., α-NH_2 (98% from eq 1), and the α-COO^- of Ala25 is charged. In contrast to the pH 2.0 results, both uWT and uS20G aggregated at pH 10.0 to form assemblies with secondary structure contents and morphologies similar to those of assemblies formed by their blocked analogues (Figure 5A for uWT and Figure 5B for uS20G). The assemblies bind ThT as indicated by the enhancement of ThT fluorescence (Figure S7).

Because the peptides contain His18, we also studied the self-assembly of uWT and uS20G at pH 7.0, above the pK_a of the residue (6.37 in IAPP(17−29)[35]) but below the pK_a of the α-NH_3^+ group. From eq 1, His18 is uncharged 80% of the time while α-NH_3^+ of Arg11 is charged 94% of the time at pH 7.0. CD spectra of uWT and uS20G at pH 7.0 and at peptide concentrations similar to those used at pH 10.0 did not change over time, indicating the absence of self-assembly (Figure S8). No enhancement of ThT fluorescence was observed, consistent with the absence of β-sheet formation (Figure S7). Together, our results obtained at pH 2.0, 4.3, 7.0, and 10.0 suggest that the restoration of the self-assembly of uncapped peptides is due to the deprotonation of α-amino group of Arg11 rather than $His18^+$.

The other titratable residue is Arg11, whose pK_a in IAPP is unknown. However, because monomeric IAPP(11−25) is predominantly random coil, its pK_a should be close to model compound values, i.e., pK_a ∼ 12.0. Thus, the residue is charged at all pH used in our experiments.

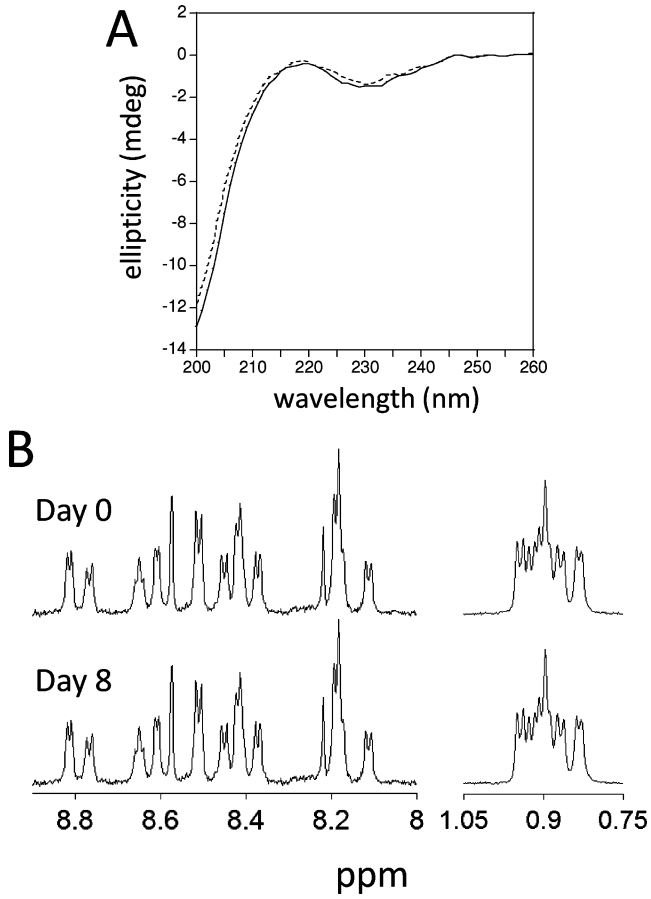

Figure 4. Removal of charge at the C-terminus of uS20G by pH titration does not restore self-assembly. (A) At pH 2.0, a condition in which the C-terminus of uS20G is protonated and neutral, the CD spectrum acquired on day 0 (solid line) is essentially identical to the spectrum acquired on day 8 (broken line). (B) 1D ^{1}H NMR spectra of uS20G also did not change with incubation time. The concentration of CD and NMR samples of uS20G is ∼60 μM.

Self-Assembly of uS20G Is Restored by Acetylation of Its N-Terminus. Another way to remove the positive charge on the α-NH_3^+ group of Arg11 is to acetylate the N-terminus of the peptide. We synthesized Ac-S20G (Figure 2) and used TEM to test for its competence for self-assembly at pH 4.3. For comparison, we also synthesized S20G-NH_2 (Figure 2). The peptides cS20G and uS20G were used as positive and negative controls, respectively. Figure 6 shows that Ac-S20G formed fibrils of indeterminate length similar to cS20G. S20G-NH_2, on the other hand, did not form fibrils.

An alternative explanation for the restoration of self-assembly upon removal of the charge on the α-NH_3^+ group of Arg11 is reduction of the net charge of the peptides which lead to reduced intermolecular electrostatic repulsion (Table S2). However, we noted that at pH 4.3 both capped and uncapped peptides (Figure 2) have a net charge of +2 (Tables S2 and S3), but only the capped peptides aggregated. Also, both Ac-S20G at pH 4.3 (Table S3) and uS20G at pH 7.0 (Table S2) have a net charge of +1, but only Ac-S20G at pH 4.3 self-assembles to fibrils.

dx.doi.org/10.1021/bi3001616 | Biochemistry 2012, 51, 4167−4174

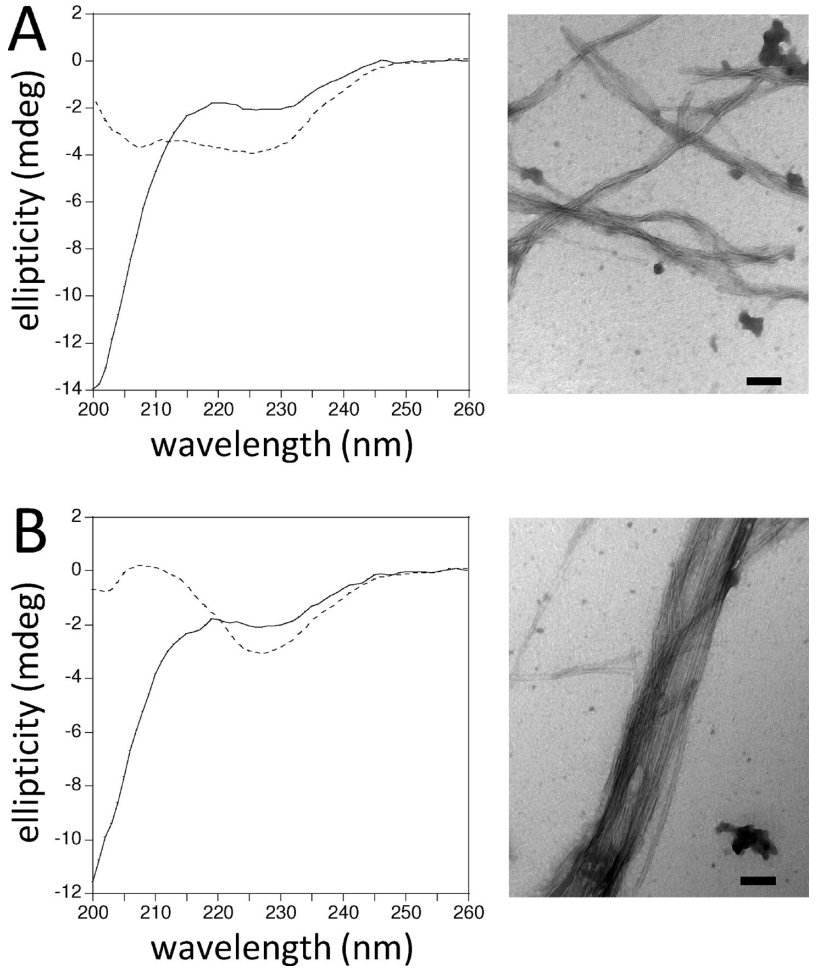

Figure 5. Removal of charge at the N-terminus of uWT and uS20G by pH titration to pH 10.0 restores self-assembly. (A) The CD spectrum of uWT acquired immediately after sample preparation (solid line) indicates random coil. The spectrum after 8 days of incubation at 4 °C (broken line) shows a minimum at 208 nm corresponding to the $\pi-\pi_{\|}^*$ transition of amide groups in an α-helix. A second minimum near 225 nm suggests the presence of some β-sheets. TEM of the day 8 CD sample shows the presence of both short and indeterminately long fibrils. Scale bar is 100 nm. (B) The CD spectrum of uS20G recorded immediately after sample preparation is consistent with a random coil conformation. After 8 days, its spectrum (broken line) shows a single minimum at 225 nm, indicating the predominant presence of β-sheet. TEM of the sample showed the presence of indeterminately long fibrils, some of which are bundled together to form thicker assemblies. Scale bar is 100 nm. The peptide concentration in both CD samples is ~60 μM.

The Helicities of the IAPP(11−25) Peptides Are Skewed toward the N-Terminus. Using a helix propensity scale based on measurements of helix propensity in 11 systems including peptides and proteins,[36] we noted that the N-terminus of IAPP(11−25) contains the three residues with the highest helical propensities, i.e., Arg^+ (Arg11), Leu (Leu12), and Ala (Ala13).[36] The C-terminus, on the other hand, contains Gly (Gly24 in wt; Gly20 and Gly24 in S20G), a helix breaker second only to proline.[36] A previous study of membrane-mediated helix formation by full-length IAPP indicates that the helical region includes residues 9−22.[14] We hypothesize therefore that the helicity of the IAPP(11−25) peptides is skewed toward the N-terminus. If true, the helix should be destabilized by the positive charge on the α-NH_3^+ group of Arg11 by helix dipole effects. The negative charge on the α-COO^- group of Ala25, on the other hand, should not affect helix stability. To test our hypothesis, we obtained CD spectra of uWT and uS20G at pH 2.0, 4.3, 7.0, and 10.0. Figure 7A shows that the dichroic spectra of uWT at pH 2.0, 4.3, and 7.0 are similar to each other. The spectrum obtained at pH 10.0, on the other hand, shows increased rotational strength in the region centered around 220 nm, suggesting an increase in helical content. Using eq 2, the helix content of uWT increases from 2% (at pH 2.0, 4.3 or 7.0) to 10% at pH 10. Similar results were obtained for uS20G (Figure S9A).

To test our hypothesis further, we performed complementary NMR studies of uWT and uS20G at pH 2.0, 4.3, 7.0, and 10.0, Ac-S20G at pH 4.3, and S20G-NH_2 at pH 4.3. After peak assignments were made, secondary chemical shifts ($\Delta\delta = \delta_{observed} - \delta_{random\ coil}$)[32] of the H^α protons which are sensitive to secondary structure were calculated and plotted against residue number (Figure 7B for uWT, Figure S9B for uS20G, Figure S10 for Ac-S20G and S20G-NH_2). Negative H^α $\Delta\delta$ values are consistent with α-helix.[37] More importantly, the magnitude of $\Delta\delta$ can be used to quantify the population of helical conformers; i.e., more negative $\Delta\delta$ values indicate a higher population of α-helical conformers.[38] We then calculated the averaged H^α $\Delta\delta$ values of residues to the left and right of His18. Because H^α chemical shifts of residues found at the N- and C-termini are sensitive to the presence of charges (α-NH_3^+ and α-COO^-) at the peptide ends,[32] we excluded Arg11 and Ala25 in our calculations. For uWT and uS20G at pH 2.0, 4.3, 7.0, and

dx.doi.org/10.1021/bi3001616 | *Biochemistry* 2012, 51, 4167−4174

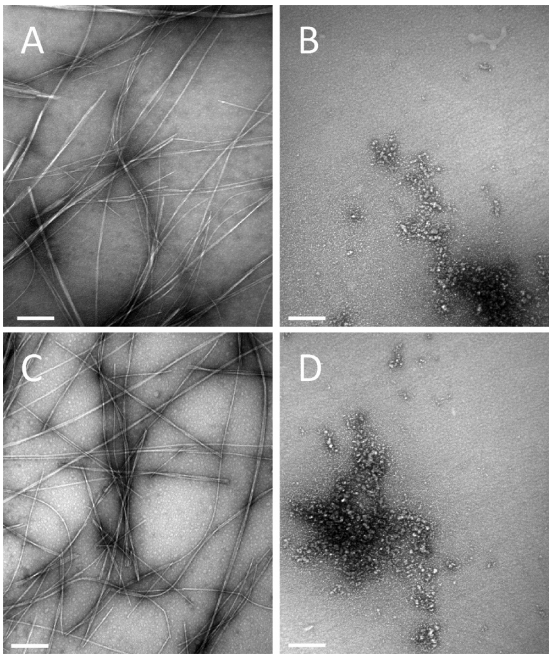

Figure 6. N-terminal acetylation of uS20G restores self-assembly to fibrils. Ac-S20G formed fibrils of indeterminate length (A) while S20G-NH_2 does not (B). Peptides cS20G (C) and uS20G (D) were used for positive and negative controls, respectively. All images were obtained after incubating the peptides at a concentration of 155 μM for 4 days at 37 °C. Bar corresponds to 100 nm.

10.0, Ac-S20G at pH 4.3, and S20G-NH_2 at pH 4.3, the average of H^{α} $\Delta\delta$ values of the residues N-terminal to His18 are more negative than those of residues C-terminal to His18 (Tables S2 and S3), consistent with our hypothesis that the helicity of IAPP(11−25) is skewed toward the N-terminus.

We also note that the $\Delta\delta$ values of Leu12 and Ala13 become more negative when the charge on the α-NH_3^+ group of Arg11 at is removed by pH titration (Figure 7B and Figure S9B) or by acetylation (Figure S10), indicating an increase in helicity of the two residues. The increase in helicity in the Leu12-Ala13 segment must result from the elimination of electrostatic repulsion between α-NH_3^+ and the positive end of the sum of the amide dipoles of the three residues. Together, these results are consistent with previous work showing that the effect of charges is limited to a few localized dipoles, i.e., confined mostly to one turn of the α-helix.[39]

Our conclusion on the effect of the α-NH_3^+ group on the helicity of the N-terminus is also supported by our investigation of helix formation by uWT and uS20G in the presence of 50% 2,2,2-trifluorethanol (TFE), an organic solvent used widely to study the helix propensity of polypeptides and proteins.[40] Results obtained by CD (Figures S11A and S11C) and NMR (Figures S11B and S11D, Table S4) for both uWT and uS20G show that helix propensity of the N-terminus increases dramatically as pH is increased from 2.0 to 10.0 and that much of the increase is localized in the Leu12-Ala13 segment (Table S5).

In summary, we show that IAPP(11−25) peptides with helicity skewed toward the N-terminus do not self-assemble when uncapped. Self-assembly is restored at pH 10.0 above the pK_a of α-NH_3^+ of Arg11 or by acetylation of the N-terminus of the peptide consistent with the removal of the destabilizing interaction between the positive charge on α-NH_3^+ and the positive end of the net dipole of the first helix turn. These results taken together with conclusions by Baldwin and others on the role of the helix dipole in α-helix stabilization[23−25] strengthen the existence of α-helical intermediates in amyloid formation.

Short, synthetic peptides have been used widely in amyloid biophysics. Both capped[41] and uncapped[42] peptides have been used. Our work suggests that one should be careful in designing experiments and interpreting results as the presence of capping groups and the protonation states of the α-amino and α-carboxyl groups may affect the ability of amyloidogenic peptides to self-assemble.

Finally, diverse lines of evidence now suggest that small, diffusible, oligomers of Aβ, α-syn, and IAPP are the proximate cytotoxic species in AD, PD, and T2D, respectively.[2−7] Oligomers may exert toxicity by membrane disruption, leading to an unregulated leakage of some cell contents, as reviewed recently.[43] The relationship between oligomer structure and toxicity has not been established primarily because of difficulties associated with the isolation and stabilization of immature assemblies for toxicity studies. Nonetheless, recent work by the Miranker group suggests that the membrane-disrupting oligomers of IAPP may be α-helix-rich, non-β-sheet assemblies.[13,44] If true, this work suggests that targeting the helix

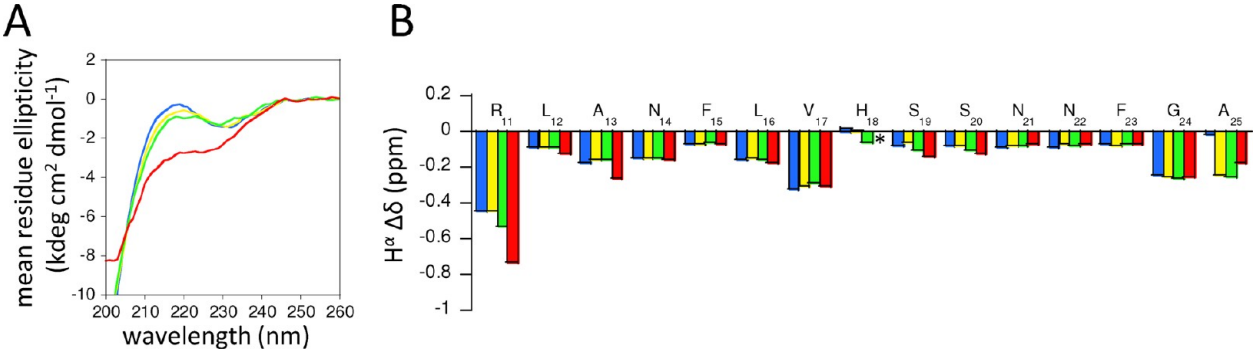

Figure 7. Deprotonation of the α-NH_3^+ group of Arg11 in uWT increases the helicity of two N-terminal residues. (A) Far-UV CD spectra of uWT at pH 2.0 (blue), pH 4.3 (yellow), pH 7.0 (green), and pH 10.0 (red) taken on day 0. At pH 10.0, an increase in mean residue ellipticity at 222 nm is observed, suggesting a higher helix content. (B) H^{α} secondary chemical shifts for uWT at pH 2.0 (blue), pH 4.3 (yellow), pH 7.0 (green), and pH 10.0 (red) plotted against residue. The $\Delta\delta$ values at pH 10.0 for Leu12 and Ala13 become more negative consistent with increased helicity in this region. The asterisk indicates that the H^{α} chemical shift of His18 at pH 10.0 cannot be determined unambiguously.

dx.doi.org/10.1021/bi3001616 | *Biochemistry* 2012, 51, 4167−4174

dipole is an attractive strategy for inhibiting the formation of α-helical oligomers.

■ ASSOCIATED CONTENT

Supporting Information

Self-assembly of cWT is abolished by removal of terminal capping groups (Figure S1); portions of the ROESY spectra of uWT and uS20G indicating the absence of ROEs between residues at the peptide ends and between His18 and residues in the C-termini of the peptides (Figures S2−S5); self-assembly of uWT is abolished at pH 2.0 (Figure S6); ThT fluorescence spectra of uncapped peptides at pH 2.0, 4.3, 7.0, and 10.0 (Figure S7); self-assembly of uWT and uS20G is abolished at pH 7.0 (Figure S8); CD spectra and secondary chemical shifts of H^{α} of uS20G in buffer at pH 2.0, 4.3, 7.0, and 10.0 (Figure S9); secondary chemical shifts of H^{α} of Ac-S20G and S20G-NH_2 peptides (Figure S10); CD spectra and secondary chemical shifts of H^{α} of uWT and uS20G in 50% TFE at pH 2.0 and 10.0 (Figure S11); electrospray-ionization mass spectrometry of uWT after 8 months of incubation at pH 2 and pH 10.0 (Figure S12); random coil shift averages from the Biological Magnetic Resonance Data Bank compare well with random coil data corrected for sequence effects (Table S1); net charge and averages of H^{α} $\Delta\delta$ of the Leu12-Val17 and Ser19-Gly24 segments of uWT and uS20G (Table S2); net charge and averages of H^{α} $\Delta\delta$ of the Ala11-Val17 and Ser19-Ala25 segments in the capped and half-capped S20G peptides at pH 4.3 (Table S3); helicity of uWT and uS20G in 50% TFE is skewed toward the N-terminus and increases when α-NH_3^+ is deprotonated (Tables S4 and S5). This material is available free of charge via the Internet at http://pubs.acs.org.

■ AUTHOR INFORMATION

Corresponding Author

*Tel (508)793-7602; Fax (508)793-8861; e-mail nlazo@clarku.edu.

Funding

This work was initially supported by a Junior Faculty Award to N.D.L. from the American Diabetes Association and by start-up funds from Clark University. V.S. was a recipient of the 2011 Lise Anne and Leo E. Beavers II Summer Undergraduate Research Fellowship.

Notes

The authors declare no competing financial interest.

■ ACKNOWLEDGMENTS

The authors thank Dr. Guoxing Lin for the maintenance of the NMR spectrometer used in this work.

■ REFERENCES

(1) Chiti, F., and Dobson, C. M. (2006) Protein misfolding, functional amyloid, and human disease. *Annu. Rev. Biochem. 75*, 333−366.

(2) Kirkitadze, M. D., Bitan, G., and Teplow, D. B. (2002) Paradigm shifts in Alzheimer's disease and other neurodegenerative disorders: The emerging role of oligomeric assemblies. *J. Neurosci. Res. 69*, 567−577.

(3) Haass, C., and Selkoe, D. J. (2007) Soluble protein oligomers in neurodegeneration: lessons from the Alzheimer's amyloid β-peptide. *Nat. Rev. Mol. Cell. Biol. 8*, 101−112.

(4) Glabe, C. G. (2008) Structural classification of toxic amyloid oligomers. *J. Biol. Chem. 283*, 29639−29643.

(5) Lansbury, P. T., and Lashuel, H. A. (2006) A century-old debate on protein aggregation and neurodegeneration enters the clinic. *Nature 443*, 774−779.

(6) Hebda, J. A., and Miranker, A. D. (2009) The interplay of catalysis and toxicity by amyloid intermediates on lipid bilayers: insights from type II diabetes. *Annu. Rev. Biophys. 38*, 125−152.

(7) Zraika, S., Hull, R. L., Verchere, C. B., Clark, A., Potter, K. J., Fraser, P. E., Raleigh, D. P., and Kahn, S. E. (2010) Toxic oligomers and islet β cell death: guilty by association or convicted by circumstantial evidence? *Diabetologia 53*, 1046−1056.

(8) Pike, C. J., Walencewicz, A. J., Glabe, C. G., and Cotman, C. W. (1991) *In vitro* aging of β-amyloid protein causes peptide aggregation and neurotoxicity. *Brain Res. 563*, 311−314.

(9) Lorenzo, A., Razzaboni, B., Weir, G. C., and Yankner, B. A. (1994) Pancreatic islet cell toxicity of amylin associated with type-2 diabetes mellitus. *Nature 368*, 756−760.

(10) Engel, M. F., Khemtemourian, L., Kleijer, C. C., Meeldijk, H. J., Jacobs, J., Verkleij, A. J., de Kruijff, B., Killian, J. A., and Hoppener, J. W. (2008) Membrane damage by human islet amyloid polypeptide through fibril growth at the membrane. *Proc. Natl. Acad. Sci. U. S. A. 105*, 6033−6038.

(11) Kirkitadze, M. D., Condron, M. M., and Teplow, D. B. (2001) Identification and characterization of key kinetic intermediates in amyloid β-protein fibrillogenesis. *J. Mol. Biol. 312*, 1103−1119.

(12) Zhu, M., Li, J., and Fink, A. L. (2003) The association of α-synuclein with membranes affects bilayer structure, stability, and fibril formation. *J. Biol. Chem. 278*, 40186−40197.

(13) Knight, J. D., Hebda, J. A., and Miranker, A. D. (2006) Conserved and cooperative assembly of membrane-bound α-helical states of islet amyloid polypeptide. *Biochemistry 45*, 9496−9508.

(14) Apostolidou, M., Jayasinghe, S. A., and Langen, R. (2008) Structure of α-helical membrane-bound human islet amyloid polypeptide and its implications for membrane-mediated misfolding. *J. Biol. Chem. 283*, 17205−17210.

(15) Abedini, A., and Raleigh, D. P. (2009) A critical assessment of the role of helical intermediates in amyloid formation by natively unfolded proteins and polypeptides. *Protein Eng., Des. Sel. 22*, 453−459.

(16) Liu, G., Prabhakar, A., Aucoin, D., Simon, M., Sparks, S., Robbins, K. J., Sheen, A., Petty, S. A., and Lazo, N. D. (2010) Mechanistic studies of peptide self-assembly: transient α-helices to stable β-sheets. *J. Am. Chem. Soc. 132*, 18223−18232.

(17) Sivanandam, V. N., Jayaraman, M., Hoop, C. L., Kodali, R., Wetzel, R., and van der Wel, P. C. (2011) The aggregation-enhancing huntingtin N-terminus is helical in amyloid fibrils. *J. Am. Chem. Soc. 133*, 4558−4566.

(18) Holzwarth, G., and Doty, P. (1965) The ultraviolet circular dichroism of polypeptides. *J. Am. Chem. Soc. 87*, 218−228.

(19) Wüthrich, K. (1986) *NMR of Proteins and Nucleic Acids*, John Wiley & Sons, New York.

(20) Fawzi, N. L., Ying, J., Torchia, D. A., and Clore, G. M. (2010) Kinetics of amyloid β monomer-to-oligomer exchange by NMR relaxation. *J. Am. Chem. Soc. 132*, 9948−9951.

(21) Wada, A. (1976) The α-helix as an electric macro-dipole. *Adv. Biophys.*, 1−63.

(22) Hol, W. G., van Duijnen, P. T., and Berendsen, H. J. (1978) The α-helix dipole and the properties of proteins. *Nature 273*, 443−446.

(23) Shoemaker, K. R., Kim, P. S., York, E. J., Stewart, J. M., and Baldwin, R. L. (1987) Tests of the helix dipole model for stabilization of α-helices. *Nature 326*, 563−567.

(24) Fairman, R., Shoemaker, K. R., York, E. J., Stewart, J. M., and Baldwin, R. L. (1989) Further studies of the helix dipole model: effects of a free α-NH3$^+$ or α-COO$^-$ group on helix stability. *Proteins 5*, 1−7.

(25) Decatur, S. M. (2000) IR spectroscopy of isotope-labeled helical peptides: probing the effect of N-acetylation on helix stability. *Biopolymers 54*, 180−185.

(26) Sakagashira, S., Sanke, T., Hanabusa, T., Shimomura, H., Ohagi, S., Kumagaye, K. Y., Nakajima, K., and Nanjo, K. (1996) Missense

mutation of amylin gene (S20G) in Japanese NIDDM patients. *Diabetes 45*, 1279−1281.
(27) Sakagashira, S., Hiddinga, H. J., Tateishi, K., Sanke, T., Hanabusa, T., Nanjo, K., and Eberhardt, N. L. (2000) S20G mutant amylin exhibits increased in vitro amyloidogenicity and increased intracellular cytotoxicity compared to wild-type amylin. *Am. J. Pathol. 157*, 2101−2109.
(28) Whitmore, L., and Wallace, B. A. (2007) Protein secondary structure analyses from circular dichroism spectroscopy: methods and reference databases. *Biopolymers 89*, 392−400.
(29) Chen, Y. H., Yang, J. T., and Chau, K. H. (1974) Determination of the helix and beta form of proteins in aqueous solution by circular dichroism. *Biochemistry 13*, 3350−3359.
(30) Lazo, N. D., and Downing, D. T. (1997) Circular dichroism of model peptides emulating the amphipathic α-helical regions of intermediate filaments. *Biochemistry 36*, 2559−2565.
(31) Cavanagh, J., Fairbrother, W. J., Palmer III, A. G., Rance, M., and Skelton, N. J. (2007) *Protein NMR Spectroscopy*, 2nd ed., Elsevier Academic Press, Amsterdam.
(32) Wishart, D. S., Sykes, B. D., and Richards, F. M. (1991) Relationship between nuclear magnetic resonance chemical shift and protein secondary structure. *J. Mol. Biol. 222*, 311−333.
(33) Schwarzinger, S., Kroon, G. J., Foss, T. R., Chung, J., Wright, P. E., and Dyson, H. J. (2001) Sequence-dependent correction of random coil NMR chemical shifts. *J. Am. Chem. Soc. 123*, 2970−2978.
(34) Kayed, R., Head, E., Thompson, J. L., McIntire, T. M., Milton, S. C., Cotman, C. W., and Glabe, C. G. (2003) Common structure of soluble amyloid oligomers implies common mechanism of pathogenesis. *Science 300*, 486−489.
(35) Mazzaglia, A., Micali, N., Scolaro, L. M., Attanasio, F., Magri, A., Pappalardo, G., and Villari, V. (2010) Aggregation properties of the peptide fragments derived from the 17−29 region of the human and rat IAPP: a comparative study with two PEG-conjugated variants of the human sequence. *J. Phys. Chem. B 114*, 705−713.
(36) Pace, C. N., and Scholtz, J. M. (1998) A helix propensity scale based on experimental studies of peptides and proteins. *Biophys. J. 75*, 422−427.
(37) Shen, Y., and Bax, A. (2007) Protein backbone chemical shifts predicted from searching a database for torsion angle and sequence homology. *J. Biomol. NMR 38*, 289−302.
(38) Wishart, D. S., and Sykes, B. D. (1994) Chemical shifts as a tool for structure determination. *Methods Enzymol. 239*, 363−392.
(39) Aqvist, J., Luecke, H., Quiocho, F. A., and Warshel, A. (1991) Dipoles localized at helix termini of proteins stabilize charges. *Proc. Natl. Acad. Sci. U. S. A. 88*, 2026−2030.
(40) Nelson, J. W., and Kallenbach, N. R. (1986) Stabilization of the ribonuclease S-peptide α-helix by trifluoroethanol. *Proteins 1*, 211−217.
(41) Madine, J., Jack, E., Stockley, P. G., Radford, S. E., Serpell, L. C., and Middleton, D. A. (2008) Structural insights into the polymorphism of amyloid-like fibrils formed by region 20−29 of amylin revealed by solid-state NMR and X-ray fiber diffraction. *J. Am. Chem. Soc. 130*, 14990−15001.
(42) Lazo, N. D., Grant, M. A., Condron, M. C., Rigby, A. C., and Teplow, D. B. (2005) On the nucleation of amyloid β-protein monomer folding. *Protein Sci. 14*, 1581−1596.
(43) Butterfield, S. M., and Lashuel, H. A. (2010) Amyloidogenic protein-membrane interactions: mechanistic insight from model systems. *Angew. Chem., Int. Ed. 49*, 5628−5654.
(44) Last, N. B., Rhoades, E., and Miranker, A. D. (2011) Islet amyloid polypeptide demonstrates a persistent capacity to disrupt membrane integrity. *Proc. Natl. Acad. Sci. U. S. A. 108*, 9460−9465.